www.czasopisma.pan.pl PAN POLSKA AKADEMIA NAUK www.journals.pan.pl

Arch. Metall. Mater. **67** (2022), 4, 1475-1479

DOI: https://doi.org/10.24425/amm.2022.141077

SE HWAN LEE[1], BYUNGMIN AHN[2*]

# SINTERING BEHAVIOR AND MECHANICAL PROPERTY OF Cu-Sn ALLOY WITH Ag ADDITION PRODUCED BY PULSED ELECTRIC CURRENT SINTERING

This work mainly focuses on the sintering behavior of the Cu-Sn alloy with the addition of Ag up to 4 wt% after pulsed electric current sintering (PECS) process for ultra-fast sintering. The microstructural evolution was characterized using scanning electron microscopy (SEM), X-ray diffraction (XRD), and density measurements. The mechanical properties were evaluated via measurements of transverse rupture strength (TRS) and Rockwell hardness. The mechanism during the sintering process has been discussed thoroughly, and the effect on porosity with the addition of the Ag is also correlated. The results showed that the growth of porosity progressed with the amount of Ag up to 2 wt%, and further addition of Ag leads reduction in porosity. The effect on mechanical properties were improved slowly as the amount of Ag increased.

*Keywords:* powder metallurgy; Cu-Sn alloy; pulsed electric current sintering; grinding tool

## 1. Introduction

Tool technologies are being widely used in various manufacturing industries that were rapidly increasing. Machining of the workpiece is divided into two main processes: cutting and grinding [1]. Cutting is a process of chip-removal such as milling and turning using inserts. Grinding is a finishing process used to improve surface roughness and tighten the tolerance on cylindrical and flat surfaces by removing a small amount of debris [2,3]. Grinding is an important process in the manufacturing of precision workpieces such as bearing, turbine blades, optics, and so on. Grinding wheels has been the subject of extensive research during high efficiency and precision machining difficult-to-cut materials in cemented carbide, Ni, or Ti base superalloy workpiece [4].

The need for grinding tools is widely increasing and the work of grinding technologies has been studied in the present. Grinding tools are divided into four major compositions which were defined as 1) metal 2) resinoid (polymer, plastic) 3) vitrified (glass) and 4) electroplated. In the case of metal-bond grinding tools, an exhibition of self-dressing capability is widely used in the machining of non-ferrous materials. Hard and brittle materials such as ceramics and stone due to the superior hardness and wear resistance [5,6]. In order to maintain high hardness and wear resistance, bonds of grinding tools are normally based on ferrous and non-ferrous alloys such as Fe, Cu, Co, Ni, Zn, and Sn. The typical bonding matrix for this group of tools includes various compositions based on either Cu, Co, or Fe [7]. The addition of Co and Fe ensures excellent tool life but deteriorates grinding performance. The tool life of metal-bond grinding tools with Cu is relatively shorter than that of grinding tools with Co and Fe, but Cu-based grinding tools exhibit good grindability and shape retention properties compared to many other grinding tools [8].

However, tools with heavy metal concentrations are potentially hazardous to the environment and health. Pb has high grinding performance and excellent liquid phase sintering (LPS) behavior. However, Pb was prohibited by the law of Restriction of Hazardous Substances (RoHS). Most countries (include European and developed countries) strictly restrict the use of Pb. Ag can be used as a substitute for the Pb which ensures excellent grinding performance, but the use of Ag is limited because of its expensive price. Cu and Ag have significant difference in melting point, density, and wetting angle. The lattice size of Cu-Ag phases is smaller than that of Cu, as a result, the volume shrinks during sintering. Therefore, when Cu-Ag phase is sintered, unlike Cu single element sintering, liquid phase sintering takes place and diffuses between the powder particles, resulting in increased sintering density [9]. In the present research, the properties of Cu-Sn grinding tools with various amount of Ag addition instead of Pb is studied in detail.

[1] AJOU UNIVERSITY, DEPARTMENT OF MATERIALS SCIENCE AND ENGINEERING AND DEPARTMENT OF ENERGY SYSTEM RESEARCH, SUWON, 16499, KOREA
[2] EHWA DIAMOND INDUSTRIAL CO., LTD., OSAN, 18145, KOREA

* Corresponding author: byungmin@ajou.ac.kr

## 2. Materials and experimental procedures

Composition of Cu-40Sn gas-atomized pre-alloyed powder (Fukuda Metal Foil & Powder, Japan) and fine Ag powder (Changsung Corporation, Korea) were mixed for 60 min in a 3-D Tubular mixer (WAB T2F, Switzerland) with Teflon mixing balls. The amount of Ag addition to the Cu-40Sn alloy was 0 to 4 wt% at 1 wt% intervals. Further, the powders are compacted in size of 40 mm × 10 mm × 4 mm at a pressure of 50 MPa using a uni-axial hydraulic press (50 ton, Korea) according to the MPIF TRS standard while using the die-wall lubricated mold.

At this work, pulsed electric current sintering (PECS, Sintris 10 STV, Italy) has been applied for the sintering process in which the specimens were heated at the rate of 100°C/min in a vacuum atmosphere. The heating included a 30-sec dwell at 430°C for de-lubrication and sintering at 600°C at 1 minute holding time. Furthermore, the phase has been evaluated by the X-ray diffractometer (Rigaku Ultima-3, Japan) (XRD, $\lambda$ = 1.540598 Å) operated at 40 kV and 40 mA. Transverse rupture strength (TRS) and Rockwell hardness (HRB, 100 kgf) were measured using a universal testing machine (Zwick/Roell UTM Z005 TN, Germany) and Rockwell hardness tester (Mitutoyo WiZhard HR-530, Japan), respectively. To assess microstructural features, Thermofisher "ChemiSEM" Axia scanning electron microscopy (SEM) was employed to detect liquid phase and microstructural evolution of sintered compacts.

## 3. Results and discussion

In Fig. 1(a), the SEM morphology has been shown. It was found that CuSn spherical-shaped powder particles have an average particle size of 30 to 40 µm. Alloy powder was evenly distributed over the examined surface during the SEM analysis while small shaped particles agglomerated over the other particle surface. While in Fig 1(b), the Ag flakes have demonstrated different shapes and thicknesses. The average length and thickness are ~10 µm and ~1 µm respectively.

In Fig. 2(a), the XRD pattern of Cu-Sn sintered alloy with and without the addition of the Ag flakes has been shown. The standard pattern has been matched with $Cu_6Sn_5$ alloy and found that the patterns are similar to the XRD pattern of $Cu_6Sn_5$ [10]. It was found that an instance peak is about 43.15° (2θ) and, several less intensity peak has been also observed without Ag added alloy. With the addition of the Ag contents, the peak intensity increased sharply up to 2 wt%. while further addition decrease and increases again. Notably, the atomic radius of the Ag (165 pm) is much higher than the Cu (145 pm) and Sn (145 pm) elements. Noticeably, it produces lattice distortion and leads to strains in the alloy system. Thus, the broadening and variation in XRD pattern could be found [11]. Moreover, the shifting of the peaks may also be possible. It is also noted that the formation of AgCu phases has been observed by the addition of the Ag element in the system. In the Cu-Ag binary phase diagram, solubility of Cu-Ag at 600°C is about 2.5 wt%, and this phase was formed up to 2 wt%. On the other hand, when the amount of Ag powers was exceed 3 wt%, supersaturated Ag atoms reacted Sn particles, and $Ag_3Sn$ intermetallic compound (IMC) phase was formed at 480°C [12]. In addition, the enthalpy of mixing of binary pairs for Cu-Sn, Cu-Ag and Sn-Ag are 7, 2 and –3 kJ/mol as per the Miedema's model. Hence, Ag-Sn is more probable to form the IMC after the addition of significant amount of Ag. Thus, a very tiny peak has been observed at 2 wt% addition of Ag, while a instance peak of AgSn has been formed due to the most negative binary pair at more than 2 wt% addition of Ag. Noticeably, the vanishing of AgCu peak has been observed due to disassociation with Ag [13]. In Fig. 2(b-f), SEM images of sintered samples have been shown. The image represents several pores on the evaluated surface along with several white precipitates. The formation of numerous pores is very obvious in the alloy after the sintering. The distribution of black pore is spread through the surface. The addition of Ag is in the alloy system increase the growth of pores simultaneously.

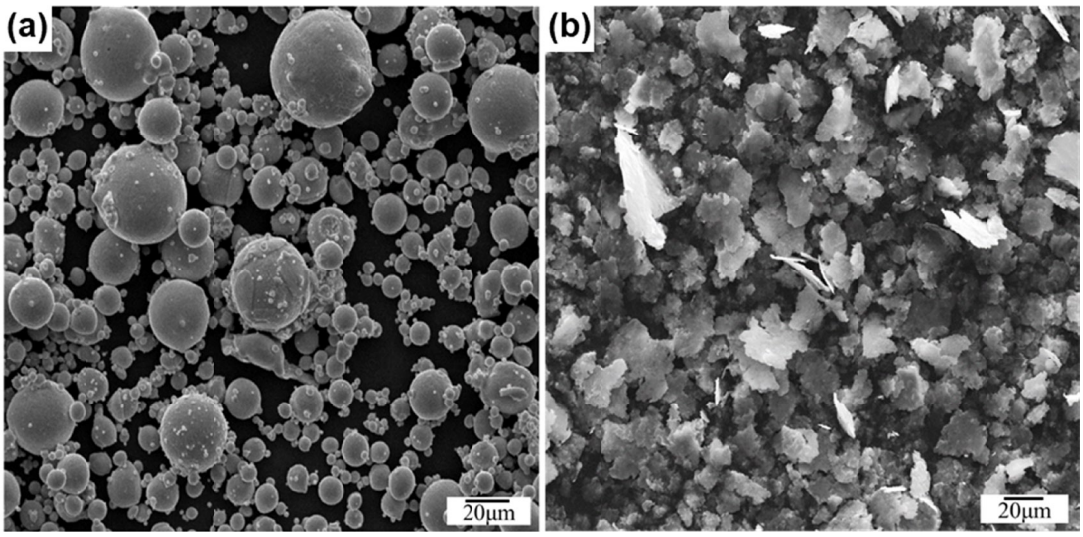


Fig. 1. SEM morphology of (a) Cu-Sn pre-alloyed powders and (b) Ag flakes

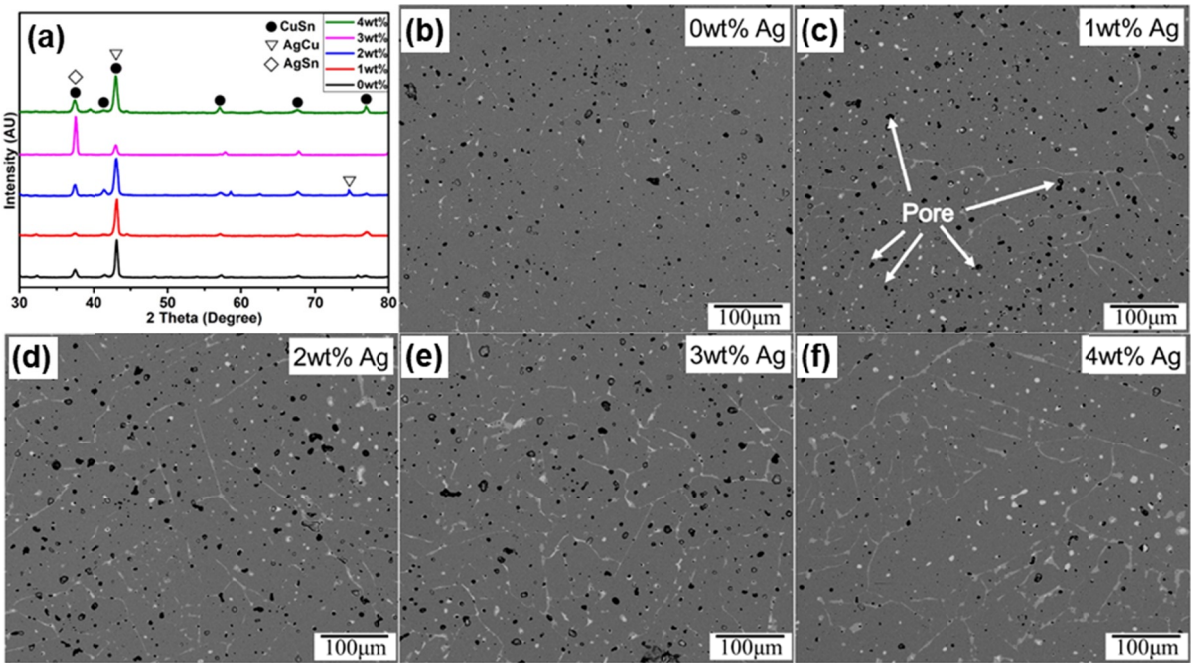


Fig. 2. (a) XRD patterns and (b-f) SEM images of Cu-40Sn with Ag addition from 0 to 4 wt%

Ag is an element of making LPS, which is a non-wetting element with 90° or more in CuO substrates or other elements [14]. When a small amount of Ag is added, the grain boundary cannot be fully packed and the liquid phase cannot be formed enough, thereby the microstructure of sintered compacts cannot make linkage and packing, which are typical shapes of LPS. Comparing the same magnification SEM micrographs of 0 wt% Ag and 1 wt% Ag, it can be seen that there is a clear difference in the pores. 1 wt%Ag sample has lots of pores than 0 wt%Ag, and the size of pores is increased than 0 wt% Ag sample.

The step-by-step formation of the alloy during the sintering has been discussed in the section. For, a better understanding of the sintering mechanism, the illustration of the mechanism and PECS equipment is shown in Fig. 3(a) and (b), respectively. The microstructural evolution that appears with the increase in Ag goes through three steps, the same as theoretical phenomena of liquid phase sintering, 1) Rearrangement of the initial state 2) Solution-reprecipitation of the intermediate state, and 3) Final densification of the final state [15].

A sufficient amount of transient liquid phase is generated in step 1, causing volume change due to movement of the liquid phase by capillary effect, and open pores in grain boundaries move and grow. Although the Ag has a poor wetting angle with a floor wettability of more than 90°, it shows a pattern of progression when it forms a sufficient liquid phase [16]. When more than 4 wt% Ag is added, the relative density reaches 99.5% or more, and it is clear that grain boundary pores are reduced even in microstructure and only intergranular pores have remained.

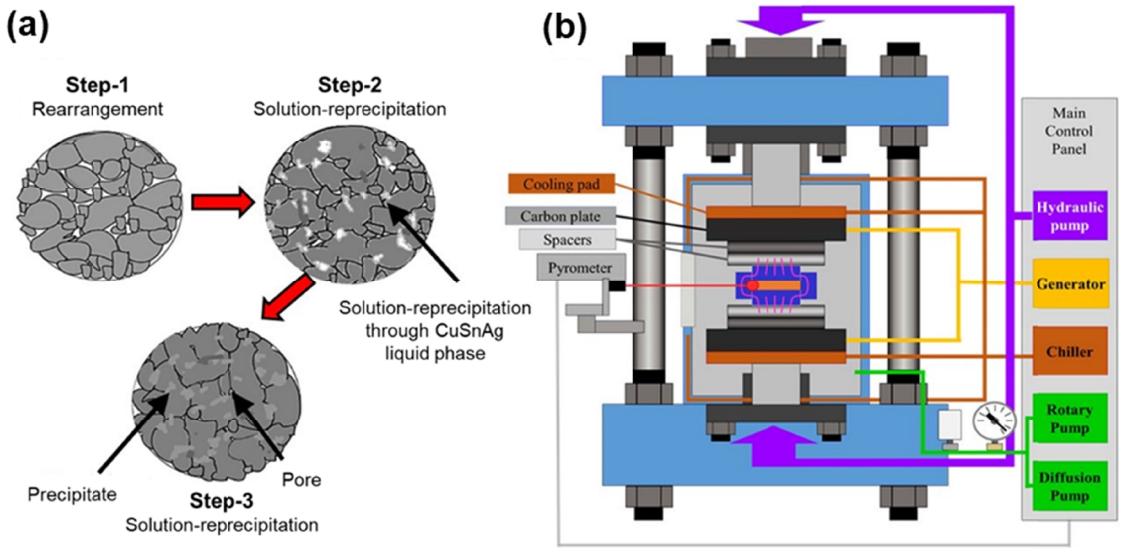


Fig. 3. (a) Step-by-step mechanism of sintering process and (b) schematic of pulsed electric current sintering (PECS) machine

Solution-precipitation in step 2 is a phenomenon in which a liquid phase is solutionized, and unlike a relatively insufficient LP appearing at 2 wt% Ag or less, sufficient LP diffuses along a grain boundary, is dissolved, and reprecipitate. In this process, the phase distribution is visible and is observed in BSE mode. The final densification, which is step 3, is a process in which the diffusion of the liquid phase is shrunk and fully densified. This is a process of increasing density through LPS, and in the case of slow rate sintering, a lot of pore movement occurs.

The density change is directly related to the durability, i.e. the life of the grinding tools [17]. When the relative density is higher, it leads to an increase of grinding tool life than low relative density. Compare to relative density, 1 wt% Ag added compact shows a noticeable actual density ($\rho$) decrease than 0 wt% Ag compact. While the addition of Ag is more than 2 wt%, it is observed that relative density is also higher than 0 wt%Ag compacts. It can be seen that when the amount of Ag added exceeds 2 wt%, the relative density increases more than the case of the 0 wt% Ag sintered sample. 1 wt% Ag is about 0.73 at%, and 2 wt% Ag is 1.46 at%. As the weight fraction of Ag increases, the total amount capable of formation of liquid phase increases to form a transitional liquid phase to proceed with LPS accompanied by linkage, and discrete pores become separator. For the microstructure perspective of the addition of Ag, the pores on the grain boundary move to form coarse pores on the grain boundary when it exceeds 3 wt% Ag. And as can be seen from the BSE image, there is a difference in phase distribution.

This experiment has a fast sintering rate of 100°C/min, the intergranular pores remain on the grain boundary without moving. In the case of 4 wt% Ag, where liquid phase is sufficiently produced, the total number of pores is less than 1-3 wt% Ag, and the relative density is also the highest. In the case of powder metallurgy, the mechanical properties of sintered compacts tend to be consistent with the density that could be seen in Fig. 4. When the sintered density is directed toward the theoretical density, compacts are sintered well and have higher mechanical properties. TRS clearly shows the interposed properties as a factor directly affected by the pore inside the compact and the neck growth of the powder.

This experiment also shows the results of matching patterns of mechanical behavior and density distribution. Both TRS and HRB decreased in the 1 wt% Ag sample where the actual density is also decreased, but both mechanical properties were incubated according to the addition of Ag. In the case of 4 wt% Ag, TRS and hardness reversed compared to 0 wt% Ag and have higher density and mechanical properties in this study. It occurs that insufficient liquid phase cannot fill the grain boundary and it leads to deteriorating mechanical properties.

This experimental condition shows a noticeable difference in the density change which is not close to theoretical density due to the increase in the addition of Ag. It is always observed that the experimental density is different from the theoretical density. It is mainly due to various experimental conditions, i.e. sintering temperature, pressure, and holding time. Isothermal sintering is difficult to reach 100% of theoretical density, and generally has a density of less than 99% even though density differences occur in the LPS process simultaneously with the shape change due to shrinkage during sintering. PECS has a unique sintering mechanism in which electric current flows through individual powders, and the temperature can be raised faster than existing isothermal sintering, and effective neck growth can occur smoothly to reach theoretical density.

## 4. Conclusions

In this study, mechanical properties according to the amount of Ag added to Cu-40Sn pre-alloyed powder were evaluated and the following conclusion has been withdrawn.

- Successfully synthesis the Cu-Sn alloy with the addition of Ag through the pulsed electric current sintering.
- When 1 wt% Ag was added, density was reduced by forming a small amount of liquid phase, but at 2 wt% Ag or more, the liquid phase is sufficiently formed to increase the density progressively.
- In the 3 wt% Ag condition, small open pores gather to form large closed pores, and the number of pores decreases while 4 wt% Ag condition, the pore linkage was shown and the

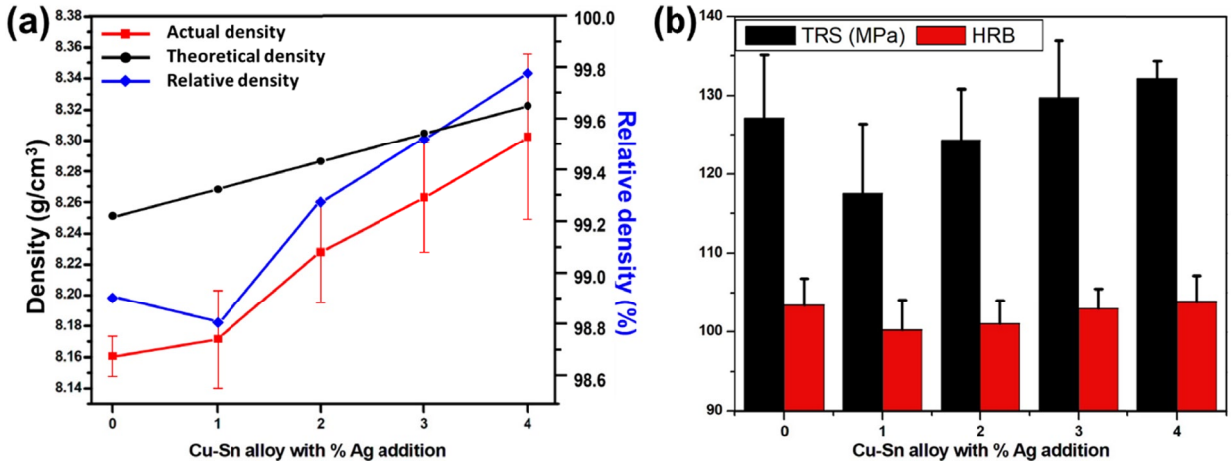


Fig. 4. (a) Sintered density and (b) transverse rupture strength (TRS) and Rockwell hardness of sintered Cu-40Sn alloy depending on Ag contents

density was satisfied by more than 99%, proving that Ag could be used instead of the existing Pb.

- As the density increases, the hardness of the sintered alloy also increases presenting a good correlation with the density and hardness.

**Acknowledgements**

This work was supported by the National Research Foundation of Korea (NRF) grant funded by the Korea government (MSIT) (No. 2021R1A2C1005478).

## REFERENCES

[1] T. Bergs, U. Müller, F. Vits, S. Barth, Diam. Relat. Mater. **108**, 107930 (2020).
[2] D. Setti, S. Ghosh, P.V. Rao, Wear **382-383**, 71 (2017).
[3] M. Tóth, N.D. Sims, D. Curtis, Procedia CIRP **82**, 214 (2019).
[4] E.E. Ibrahim, M. Checkley, X. Chen, M. Sharp, W. Liang, S. Yuan, A.D.L. Batako, Procedia Manuf. **30**, 530 (2019).
[5] P.A. Loginov, D.A. Sidorenko, E.A. Levashov, M.I. Petrzhik, M.Y. Bychkova, L. Mishnaevsky Jr., Int. J. Refract. Hard Met. **71**, 36 (2018).
[6] J.-W. Peng, F.-L. Zhang, Y.-J. Huang, J.-M. Liu, K.-J. Li, Y.-M. Zhou, Y. Long, C.-Y. Wang, S.-H. Wu, H.-Q. Tang, Ceram. Int. **47**, 32736 (2021).
[7] Y. Li, H. Zhou, C. Wu, Z. Yin, C. Liu, Y. Huang, J. Liu, Z. Shi, Metals **11**, 196 (2021).
[8] A. Seleznev, N.W.S. Pinargote, A. Smirnov, Metals **11**, 1385 (2021).
[9] R. Sayyadi, F. Khodabakhshi, N.S. Javid, G. Khatibi, J. Mater. Res. Technol. **9**, 8953(2020).
[10] Z. Zhang, C. Wei, H. Cao, Y. Zhang, Materials **12**, 4127 (2019).
[11] S. Guo, C. Ng, C.T. Liu, J. Alloys Compd. **557**, 77 (2013).
[12] C.-S. Oh, J.-H. Shim, B.-J. Lee and D.N. Lee, J. Alloys & Compds. **238**, 155 (1996).
[13] M.S. Mousavi, R. Abbasi, S.F. Kashani-Bozorg, Metall. Mater. Trans. A **47**, 3761 (2016).
[14] Y. Grosu, L. González-Fernández, U. Nithiyanantham, A. Faik, Energies **12**, 3765 (2019).
[15] R. Collet, S.L. Gallet, F. Charlot, S. Lay, J.-M. Chaix, F. Bernard, J. Manuf. Mater. Process. **5**, 119 (2021).
[16] N. Eustathopoulos, Metals **5**, 350 (2015).
[17] S. Zhang, K. Zhou, H. Ding, J. Guo, Q. Liu, W. Wang, Materials **11**, 2293 (2018).